Nanotechnology **22** (2011) 285702 (5pp) doi:10.1088/0957-4484/22/28/285702

Time-dependent density functional study of field emission from nanotubes composed of C, BN, SiC, Si, and GaN

Joseph A Driscoll[1], **Sergiy Bubin**[1], **William R French**[2] **and Kalman Varga**[1]

[1] Department of Physics and Astronomy, Vanderbilt University, Nashville, TN 37235, USA
[2] Department of Chemical and Biomolecular Engineering, Vanderbilt University, Nashville, TN 37235, USA

E-mail: joseph.a.driscoll@vanderbilt.edu

Received 15 March 2011, in final form 3 May 2011
Published 6 June 2011
Online at stacks.iop.org/Nano/22/285702

Abstract
Field emission from various types of nanotubes is studied by propagating the electronic density in real space and time using time-dependent density functional theory. Capped (5, 5) C, BN, SiC, Si, and GaN nanotubes are considered. The GaN, SiC, and Si nanotubes were found to be significantly better field emitters than C and BN nanotubes, both in terms of current magnitude and sharpness of peaks in the energy spectra. By analyzing the electronic structure of the various systems it is seen that the nanotubes with the highest currents have electron densities that extend significantly from the nanotube in the emission direction.

(Some figures in this article are in colour only in the electronic version)

The high aspect ratio and atomically sharp apex make carbon nanotubes (CNTs) ideal for applications as field emitters. In addition to these geometrical features, CNTs have high electrical and thermal conductivity and high chemical and thermal stability which allows the fabrication of novel CNT-based devices such as next-generation displays [1–6], electron sources [7–9], and high-resolution electron beam instruments [10–12]. In addition to carbon, nanotubes of other types have also been synthesized which share some of the same desirable properties of CNTs. Examples include BN [13], SiC [14], Si [15], and GaN [16].

In this paper the field emission of BN, C, SiC, Si, and GaN nanotubes is investigated using time-dependent density functional theory (TDDFT) [17]. We will study how the intensity and energy resolution of the emitted electrons depend on the composition and on the electronic structure of the field emitter. The results show that different kinds of nanotubes have significantly different field emission strengths.

The first theoretical studies of field emission date back to the early days of quantum mechanics. The standard approach to modeling field emission is the Fowler–Nordheim (FN) theory [18] which describes the emission of electrons from a flat metal surface in the presence of an electric field. More rigorous methods that take into account atomic geometry and electronic structure have been developed in recent years [19–22] and include first-principles approaches. These approaches involve the calculation of the self-consistent electronic structure of the field emitter and connect the wavefunction to the asymptotic scattering wavefunction of the electrons in the external field [20, 21]. An important step beyond these static calculations is the introduction of the time-dependent description of FE [23, 24]. The time-dependent description so far has been limited to time propagation of the wavefunctions with a time-independent ground state Hamiltonian.

The present work goes beyond previous time-dependent approaches [23, 24] and simulates the entire field emission process in a real-time, real-space framework. In the time-dependent approach the wavefunction is time propagated to describe the effect of the electric field. This approach has several advantages. In the time-independent approach, the wavefunction has to be matched to the asymptotic wavefunction. The asymptotic wavefunction, the wavefunction of electrons in an electric field, is not known. It is usually approximated by Airy functions, the wavefunctions of independent, non-interacting electrons in an electric field.

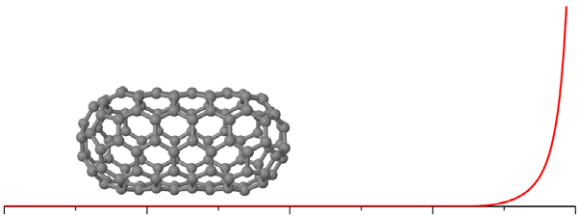

Figure 1. Use of a complex potential in a field emission calculation. The imaginary potential absorbs the electronic density in the asymptotic region, preventing reflections.

This approximation is avoided in the time-dependent approach: the field-emitted electrons and the charge redistribution in the nanotubes are described on an equal footing. The asymptotic form of the wavefunction is not needed in the calculation, and the time evolution of the wavefunction is used to describe the emitted current.

In the TDDFT framework [17] the electronic motion is described by the following time-dependent Kohn–Sham equation for single particle orbitals Ψ_i:

$$\mathrm{i}\hbar\frac{\partial}{\partial t}\Psi_i(\mathbf{r},t) = H\Psi_i(\mathbf{r},t) \tag{1}$$

with

$$H = H_{\mathrm{KS}} + V_{\mathrm{ext}} \tag{2}$$

$$H_{\mathrm{KS}} = -\frac{\hbar^2}{2m}\nabla_{\mathbf{r}} + V_{\mathrm{A}}(\mathbf{r},t) + V_{\mathrm{H}}[\rho](\mathbf{r},t) + V_{\mathrm{XC}}[\rho](\mathbf{r},t), \tag{3}$$

where $V_{\mathrm{ext}}(\mathbf{r},t)$ is the time-dependent external potential, $V_{\mathrm{A}}(\mathbf{r},t)$ is the atomic potential, $V_{\mathrm{H}}(\mathbf{r},t)$ is the Hartree potential, and $V_{\mathrm{XC}}(\mathbf{r},t)$ is the exchange–correlation potential. To represent $V_{\mathrm{A}}(\mathbf{r},t)$ we used pseudopotentials [25]. The exchange–correlation potential $V_{\mathrm{XC}}(\mathbf{r},t)$ is constructed using the adiabatic local density approximation [26] and the Hartree potential is calculated by solving the Poisson equation. The electron charge density is given by $\rho(\mathbf{r},t) = \sum_i |\Psi_i(\mathbf{r},t)|^2$ and the current is defined as

$$\mathbf{j}(\mathbf{r},t) = \frac{e\hbar}{2\mathrm{i}m}\sum_i(\Psi_i^*\nabla_{\mathbf{r}}\Psi_i - \Psi_i\nabla_{\mathbf{r}}\Psi_i^*). \tag{4}$$

One difficulty in time-dependent calculations arises from the finite size of the simulation volume. Typically, long simulation times are needed for the system to reach a steady state in which measurements can be made. In a finite simulation volume, however, long simulations allow the electron density to reach the end of the volume and produce non-physical reflections. To avoid artificial reflections from the boundaries during the time evolution we used complex absorbing potentials (CAPs) near the boundaries. The CAP absorbs the outgoing waves and so prevents reflections from the boundaries. Figure 1 shows the arrangement of the system. The CAP is zero near the nanotube, and so does not impact calculations of the current. In this work we used the form of a CAP taken from Manolopoulos [27]. It gradually increases to infinity at the right end of the simulation volume.

The time-dependent Kohn–Sham equation (1) is solved by time propagating the Kohn–Sham orbitals. The Taylor propagator [28] is used for the time development of the wavefunction:

$$\Psi_k(\mathbf{r},t+\Delta t) = \sum_{j=0}^{N_{\mathrm{T}}}\frac{(\mathrm{i}\hbar)^j}{j!}H^j\Psi_k(\mathbf{r},t), \tag{5}$$

where the order of the Taylor expansion is taken to be $N_{\mathrm{T}} = 4$. The system's ground state is used for the initial state $\Psi_k(\mathbf{r}, t = 0)$. The time-dependent Hamiltonian is the sum of the Kohn–Sham Hamiltonian H_{KS}, the Hamiltonian of the interaction with the electric field $V_E = -eEx$, and the left/right absorbing potentials W_{L} and W_{R}, giving $H = H_{\mathrm{KS}}(t) + V_E + W_{\mathrm{L}} + W_{\mathrm{R}}$. The time-dependent density functional calculations presented here are implemented using our Lagrange function [29] based on real-space, real-time code. Our use of a real-space grid basis allows representation of all types of electron orbitals including s, p, d, etc states.

It is important to note that the calculations presented here incorporate the effects of space charge [30, 31] and the Boersch effect [32] (broadening of the electron beam's energy spread due to the interaction between electrons within the emitted beam). This is because for each time step we calculate the electron density, and solve the Poisson equation to get the resulting potential. As a result, any space charge or Boersch effects will be included, and no *ad hoc* modeling is required.

It is known [33–36] that nanotubes can assume different geometries. In order to see the differences in field emission properties caused by changes in composition, we kept other aspects of the nanotubes the same. They all had (5, 5) chirality, end caps made from half-C60 molecules, and a total of 120 atoms per nanotube.

To generate realistic coordinates for the various nanotubes, we performed classical molecular dynamics (MD) simulations using the Tersoff potential [37]. Parameters were taken from [38, 39] for C, [40] for Si and SiC, and [41, 42] for BN. Reference [43] was used for the GaN structure. The Tersoff potential is an empirical interatomic potential that has been widely used to study the properties of semiconducting materials [37, 38, 40]. Through the incorporation of information about bond order in an atom's local environment, the Tersoff potential describes electronic structure effects (e.g. sp^3 bonding) more explicitly than conventional pairwise potentials. Its accuracy has been demonstrated through numerous forms of property prediction, ranging from lattice and elastic constants for crystalline structures [38, 40] to cohesive energies [44] and mechanical behavior [45–47] for nanotubes.

In carrying out the MD simulations, we utilized the LAMMPS [48] open source package with a time step of 2.0 fs and the equations of motion were integrated via the standard velocity Verlet algorithm. The simulations were performed in the canonical (constant NVT) ensemble with the Nosé–Hoover thermostat applied. To produce the final relaxed coordinates, the following annealing procedure was used: (i) run MD for 100 ps at 298 K, (ii) run MD for 100 ps while ramping the temperature down from 298 to 0 K, (iii) run MD for 50 ps at 0 K.

After the geometry of the nanotubes was optimized, the ground state orbitals $\Psi_k(\mathbf{r}, t = 0)$ were calculated by solving

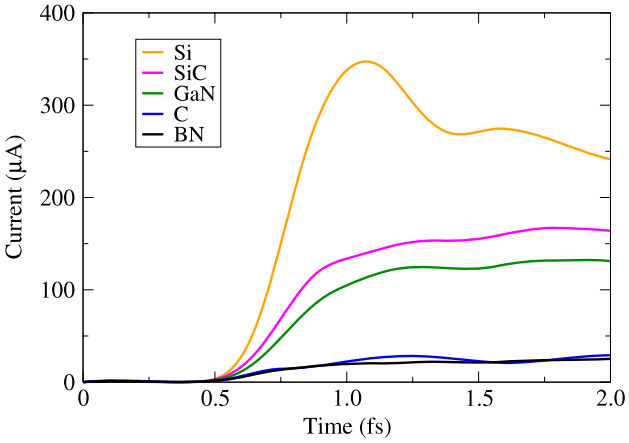

Figure 2. Current versus time for nanotubes of varying composition at a field strength of 1.00 V Å^{-1}.

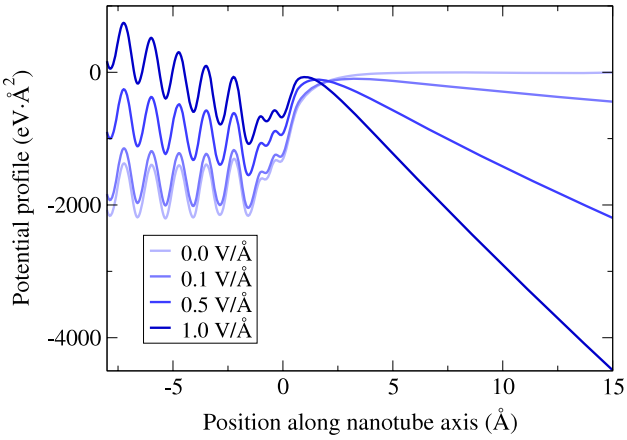

Figure 3. Potential profile for 120 atom C nanotube at different electric field strengths.

Table 1. Peak field emission currents (in μA) for (5, 5) capped nanotubes with differing composition in varying electric fields.

	0.10 V Å^{-1}	0.50 V Å^{-1}	1.00 V Å^{-1}
C	0.024	1.297	29.384
BN	0.029	2.561	32.916
GaN	0.076	7.844	132.279
SiC	0.085	9.259	167.105
Si	0.162	28.292	347.537

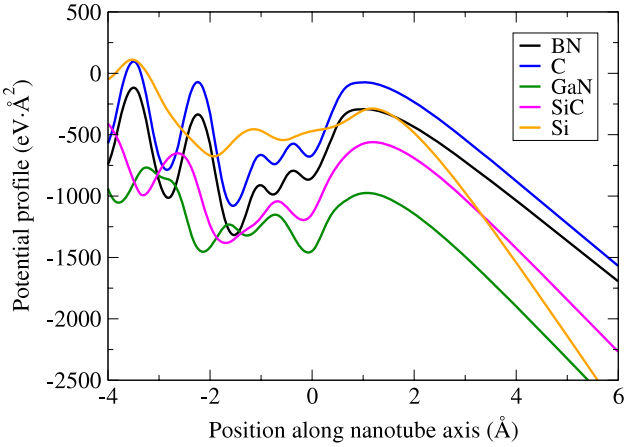

Figure 4. Potential profile for various nanotubes at the field strength of 1.00 V Å^{-1}.

the self-consistent Kohn–Sham equations. Once the ground state of the system is obtained, the electric field is turned on and time development for a few femtoseconds begins. The electric field's magnitude is increased slowly with a linear ramp over 0.1 fs. Once a steady state has been reached, the FE current is calculated using (4) (see table 1).

Due to the high computational cost of the calculations, the size of the nanotubes is limited to 120 atoms. Once the electric field is turned on and the field emission starts, the nanotubes become charged due to the loss of electrons. This limits the length of the simulation time; once the electron deficiency of the nanotube becomes too large the field emission decreases (see figure 2). It should also be noted that increasing the number of atoms in a nanotube results in a somewhat increased current. Apparently, very long nanotubes are necessary in order to obtain completely converged values for the current magnitude, but this is computationally impractical. The aim of the present simulations, however, is to study how the composition of the nanotubes affects their field emission properties. Since we keep the same number of atoms (and electrons) in all of our structures, it allows us to make a meaningful comparison.

The calculated currents for different electric fields are shown in table 1. The electric fields used in these calculations span the typical range of fields used in field emission experiments. The GaN, SiC, and Si nanotubes have much larger currents than the other nanotubes. BN and C nanotubes have similar current values, with BN being slightly higher.

Figure 3 shows the profile of the local part of the potential in the direction of the electric field (x-axis) for different electric field magnitudes (by profile we mean the local potential integrated in the yz plane; i.e. it is a projection onto the x-axis). For higher electric fields the potential barrier lowers and gets narrower allowing higher electron currents. In the present calculations the core electrons are replaced by pseudopotentials which consist of both local and nonlocal parts. The use of nonlocal pseudopotentials makes the qualitative analysis of the potential profiles difficult. We cannot directly compare the potential distribution of nanotubes to study the reasons behind the differences in field emission currents because for different elements the contributions from the local and nonlocal parts differ.

In figure 4 the potential profile is plotted for the various nanotubes in the case of 1.00 V Å^{-1} field strength. It should be emphasized once again that this is an approximate picture, which lacks the contribution from the nonlocal part of the potential and does not show the full 3D structure of the total potential. Nonetheless, it serves as a good illustration of the basic mechanism that controls the field emission properties of various structures. As can be seen in figure 4 the potential barrier height and width for a given nanotube correlates quite well with the actual current intensity.

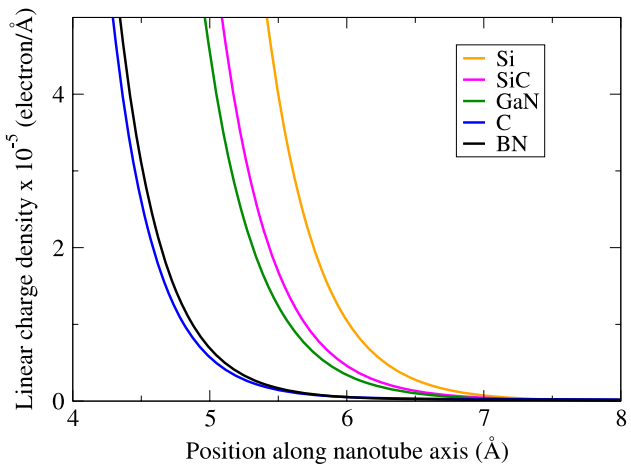

Figure 5. Density profile for the different nanotubes at the field strength of 1.00 V Å^{-1}.

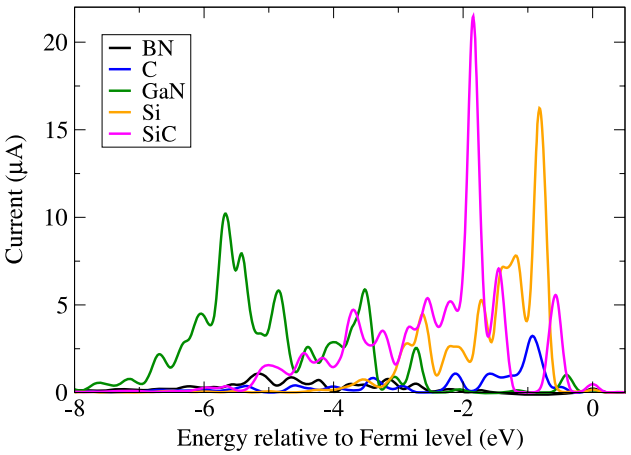

Figure 6. Current versus energy, relative to Fermi energy at a field strength of 1.00 V Å^{-1}. The spectral peaks were broadened with Gaussians, using a full width at half maximum of 0.2 eV.

The density profile for the various nanotubes is shown in figure 5. This shows that for some of the nanotubes, the electron density extends further from the tube. From table 1 we see that this correlates with higher currents.

Figure 6 shows the current versus energy distribution for the different nanotubes. The most intriguing feature of this figure is that the current is not emitted from one high lying orbital but instead originates from several states below the Fermi energy.

In summary, the field emissions from nanotubes of various composition have been studied using time-dependent density functional theory. The calculations predict that the GaN, SiC, and Si nanotubes are particularly good field emitters. The highest-current nanotube, Si, is predicted to produce a current an order of magnitude higher than BN or C nanotubes.

Acknowledgment

This work has been supported by NSF Grant CMMI0927345.

References

[1] Choi W B, Chung D S, Kang J H, Kim H Y, Jin Y W, Han I T, Lee Y H, Jung J E, Lee N S and Park G S 1999 Fully sealed, high-brightness carbon-nanotube field-emission display *Appl. Phys. Lett.* **75** 3129

[2] Saito Y and Uemura S 2000 Field emission from carbon nanotubes and its application to electron sources *Carbon* **38** 169–82

[3] Wang Q H, Setlur A A, Lauerhaas J M, Dai J Y, Seelig E W and Chang R P H 1998 A nanotube-based field-emission flat panel display *Appl. Phys. Lett.* **72** 2912

[4] Wang Q H, Yan M and Chang R P H 2001 Flat panel display prototype using gated carbon nanotube field emitters *Appl. Phys. Lett.* **78** 1294–6

[5] Bonard J-M, Stöckli T, Noury O and Châtelain A 2001 Field emission from cylindrical carbon nanotube cathodes: possibilities for luminescent tubes *Appl. Phys. Lett.* **78** 2775–7

[6] Mauger M and Binh V T 2006 Vertically aligned carbon nanotube arrays for giant field emission displays *J. Vac. Sci. Technol.* B **24** 997–1003

[7] de Heer W A, Châtelain A and Ugarte D 1995 A carbon nanotube field-emission electron source *Science* **270** 1179

[8] Saito Y, Hamaguchi K, Hata K, Uchida K, Tasaka Y, Ikazaki F, Yumura M, Kasuya A and Nishina Y 1997 Conical beams from open nanotubes *Nature* **389** 554

[9] Rinzler A G, Hafner J H, Nikolaev P, Nordlander P, Colbert D T, Smalley R E, Lou L, Kim S G and Tomanek D 1995 Unraveling nanotubes: field emission from an atomic wire *Science* **269** 1550–3

[10] Dean K A and Chalamala B R 1999 Field emission microscopy of carbon nanotube caps *J. Appl. Phys.* **85** 3832–6

[11] de Jonge N, Lamy Y, Schoots K and Oosterkamp T H 2002 High brightness electron beam from a multi-walled carbon nanotube *Nature* **420** 393–5

[12] Schmid H and Fink H-W 1997 Carbon nanotubes are coherent electron sources *Appl. Phys. Lett.* **70** 2679–80

[13] Chopra N G, Luyken R J, Cherrey K, Crespi V H, Cohen M L, Louie S G and Zettl A 1995 Boron nitride nanotubes *Science* **269** 966–7

[14] Sun X-H, Li C-P, Wong W-K, Wong N-B, Lee C-S, Lee S-T and Teo B-K 2002 Formation of silicon carbide nanotubes and nanowires via reaction of silicon (from disproportionation of silicon monoxide) with carbon nanotubes *J. Am. Chem. Soc.* **124** 14464–71

[15] Sha J, Niu J, Ma X, Xu J, Zhang X, Yang Q and Yang D 2002 Silicon nanotubes *Adv. Mater.* **14** 1219–21

[16] Goldberger J, He R, Zhang Y, Lee S, Yan H, Choi H J and Yang P 2003 Single-crystal gallium nitride nanotubes *Nature* **422** 599–602

[17] Runge E and Gross E K U 1984 Density-functional theory for time-dependent systems *Phys. Rev. Lett.* **52** 997–1000

[18] Fowler R H and Nordheim L 1928 Electron emission in intense electric fields *Proc. Phys. Soc. London* A **119** 173–81

[19] Jensen K L 1999 Exchange–correlation, dipole, and image charge potentials for electron sources: temperature and field variation of the barrier height *J. Appl. Phys.* **85** 2667–80

[20] Lang N D, Yacoby A and Imry Y 1989 Theory of a single-atom point source for electrons *Phys. Rev. Lett.* **63** 1499–502

[21] Gohda Y, Nakamura Y, Watanabe K and Watanabe S 2000 Self-consistent density functional calculation of field emission currents from metals *Phys. Rev. Lett.* **85** 1750–3

[22] Maiti A, Andzelm J, Tanpipat N and von Allmen P 2001 Effect of adsorbates on field emission from carbon nanotubes *Phys. Rev. Lett.* **87** 155502

[23] Han S, Lee M H and Ihm J 2002 Dynamical simulation of field emission in nanostructures *Phys. Rev.* B **65** 085405

[24] Tada K and Watanabe K 2002 *Ab initio* study of field emission from graphitic ribbons *Phys. Rev. Lett.* **88** 127601

[25] Troullier N and José L M 1991 Efficient pseudopotentials for plane-wave calculations *Phys. Rev.* B **43** 1993–2006
[26] Gross E K U and Kohn W 1985 Local density-functional theory of frequency-dependent linear response *Phys. Rev. Lett.* **55** 2850–2
[27] Manolopoulos D E 2002 Derivation and reflection properties of a transmission-free absorbing potential *J. Chem. Phys.* **117** 9552–9
[28] Yabana K and Bertsch G F 1996 Time-dependent local-density approximation in real time *Phys. Rev.* B **54** 4484–7
[29] Varga K, Zhang Z and Pantelides S T 2004 Lagrange functions: a family of powerful basis sets for real-space order-n electronic structure calculations *Phys. Rev. Lett.* **93** 176403
[30] Barbour J P, Dolan W W, Trolan J K, Martin E E and Dyke W P 1953 Space–charge effects in field emission *Phys. Rev.* **92** 45–51
[31] Bonard J-M, Salvetat J-P, Stöckli T, de Heer W A, Forró L and Châtelain A 1998 Field emission from single-wall carbon nanotube films *Appl. Phys. Lett.* **73** 918–20
[32] Boersch H 1954 Experimentelle bestimmung der energieverteilung in thermisch ausgelösten elektronenstrahlen *Z. Phys.* **139** 115–46
[33] Ayala P, Arenal R, Loiseau A, Rubio A and Pichler T 2010 The physical and chemical properties of heteronanotubes *Rev. Mod. Phys.* **82** 1843–85
[34] Blase X, De Vita A, Charlier J-C and Car R 1998 Frustration effects and microscopic growth mechanisms for bn nanotubes *Phys. Rev. Lett.* **80** 1666–9
[35] Zhang Y and Huang H 2008 Stability of single-wall silicon carbide nanotubes—molecular dynamics simulations *Comput. Mater. Sci.* **43** 664–9
[36] Bunder J E and Hill J M 2009 Electronic properties of silicon nanotubes with distinct bond lengths *Phys. Rev.* B **79** 233401
[37] Tersoff J 1988 New empirical approach for the structure and energy of covalent systems *Phys. Rev.* B **37** 6991–7000
[38] Tersoff J 1988 Empirical interatomic potential for carbon, with applications to amorphous carbon *Phys. Rev. Lett.* **61** 2879–82
[39] Lindsay L and Broido D A 2010 Optimized tersoff and brenner empirical potential parameters for lattice dynamics and phonon thermal transport in carbon nanotubes and graphene *Phys. Rev.* B **81** 205441
[40] Tersoff J 1989 Modeling solid-state chemistry: interatomic potentials for multicomponent systems *Phys. Rev.* B **39** 5566–8
[41] Sekkal W, Bouhafs B, Aourag H and Certier M 1998 Molecular-dynamics simulation of structural and thermodynamic properties of boron nitride *J. Phys.: Condens. Matter* **10** 4975
[42] Verma V, Jindal V K and Dharamvir K 2007 Elastic moduli of a boron nitride nanotube *Nanotechnology* **18** 435711
[43] Benkabou F, Certier M and Aourag H 2003 Elastic properties of zinc-blende g a n, a l n and i n n from molecular dynamics *Mol. Simulation* **29** 201–9
[44] Sawada S and Hamada N 1992 Energetics of carbon nano-tubes *Solid State Commun.* **83** 917–9
[45] Wang Z, Zu X, Gao F and Weber W J 2008 Atomistic simulations of the mechanical properties of silicon carbide nanowires *Phys. Rev.* B **77** 224113
[46] Zhou R L, Wang L and Pan B C 2010 Elastic and melting properties of crystalline SiC nanotubes *J. Phys. Chem.* C **114** 8199–205
[47] Setoodeh A R, Jahanshahi M and Attariani H 2009 Atomistic simulations of the buckling behavior of perfect and defective silicon carbide nanotubes *Comput. Mater. Sci.* **47** 388–97
[48] Plimpton S 1995 Fast parallel algorithms for short-range molecular dynamics *J. Comput. Phys.* **117** 1–19